Generalized-ICP

Aleksandr V. Segal
Stanford University
Email: avsegal@cs.stanford.edu

Dirk Haehnel
Stanford University
Email: haehnel@stanford.edu

Sebastian Thrun
Stanford University
Email: thrun@stanford.edu

Abstract— In this paper we combine the Iterative Closest Point ('ICP') and 'point-to-plane ICP' algorithms into a single probabilistic framework. We then use this framework to model locally planar surface structure from both scans instead of just the "model" scan as is typically done with the point-to-plane method. This can be thought of as 'plane-to-plane'. The new approach is tested with both simulated and real-world data and is shown to outperform both standard ICP and point-to-plane. Furthermore, the new approach is shown to be more robust to incorrect correspondences, and thus makes it easier to tune the maximum match distance parameter present in most variants of ICP. In addition to the demonstrated performance improvement, the proposed model allows for more expressive probabilistic models to be incorporated into the ICP framework. While maintaining the speed and simplicity of ICP, the Generalized-ICP could also allow for the addition of outlier terms, measurement noise, and other probabilistic techniques to increase robustness.

I. INTRODUCTION

Over the last decade, range images have grown in popularity and found increasing applications in fields including medical imaging, object modeling, and robotics. Because of occlusion and limited sensor range, most of these applications require accurate methods of combining multiple range images into a single model. Particularly in mobile robotics, the availability of range sensors capable of quickly capturing an entire 3D scene has drastically improved the state of the art. A striking illustration of this is the fact that virtually all competitors in the DARPA Grand Challenge relied on fast-scanning laser range finders as the primary input method for obstacle avoidance, motion planning, and mapping. Although GPS and IMUs are often used to calculate approximate displacements, they are not accurate enough to reliably produce precise positioning. In addition, there are many situation (tunnels, parking garages, tall buildings) which obstruct GPS reception and further decrease accuracy. To deal with this shortcoming, most applications rely on scan-matching of range data to refine the localization. Despite such wide usage, the typical approach to solving the scan-matching problem has remained largely unchanged since its introduction.

II. SCANMATCHING

Originally applied to scan-matching in the early 90s, the ICP technique has had many variations proposed over the past decade and a half. Three papers published around the same time period outline what is still considered the state of the art solution for scan-matching. The most often cited analysis of the algorithm comes from Besl and McKay[1]. [1] directly addresses registration of 3D shapes described either geometrically or with point clouds. Chen and Medioni[7] considered the more specific problem of aligning range data for object modeling. Their approach takes advantage of the tendency of most range data to be locally planar and introduces the "point-to-plane" variant of ICP. Zhang[5] almost simultaneously describes ICP, but adds a robust method of outlier rejection in the correspondence selection phase of the algorithm.

Two more modern alternatives are Iterative Dual Correspondence [15] and Metric-Based ICP [16]. IDC improves the point-matching process by maintaining two sets of correspondences. MbICP is designed to improve convergence with large initial orientation errors by explicitly putting a measure of rotational error as part of the distance metric to be minimized.

The primary advantages of most ICP based methods are simplicity and relatively quick performance when implemented with kd-trees for closest-point look up. The drawbacks include the implicit assumption of full overlap of the shapes being matched and the theoretical requirement that the points are taken from a known geometric surface rather than measured [1]. The first assumption is violated by partially overlapped scans (taken from different locations). The second causes problems because different discretizations of the physical surface make it impossible to get exact overlap of the individual points even after convergence. Point-to-plane, as suggested in [7], solves the discretization problem by not penalizing offsets along a surface. The full overlap assumption is usually handled by setting a maximum distance threshold in the correspondence.

Aside from point-to-plane, most ICP variations use a closed form solution to iteratively compute the alignment from the correspondences. This is typically done with [10] or similar techniques based on cross-correlation of the two data sets. Recently, there has been interest in the use of generic non-linear optimization techniques instead of the more specific closed form approaches [9]. These techniques are advantageous in that they allow for more generic minimization functions rather then just the sum of euclidean distances. [9] uses non-linear optimization with robust statistics to show a wider basin of convergence.

We argue that among these, the probabilistic techniques are some of the best motivated due to the large amount of theoretical work already in place to support them. [2] applies a probabilistic model by assuming the second scan is generated from the first through a random process. [4] Applies ray tracing techniques to maximize the probability of alignment.

[8] builds a set of compatible correspondences, and then maximizes probability of alignment over this distribution. [17] introduces a fully probabilistic framework which takes into account a motion model and allows estimates of registration uncertainty. An interesting aspect of the approach is that a sampled analog of the Generalized Hough Transform is used to compute alignment without explicit correspondences, taking both surface normals into account for 2D data sets.

There is also a large amount of literature devoted to solving the global alignment problem with multiple scans ([18] and many others). Many approaches to this ([18] in particular) use a pair-wise matching algorithm as a basic component. This makes improvements in pairwise matching applicable to the global alignment problem as well.

Our approach falls somewhere between standard IPC and the fully probabilistic models. It is based on using MLE as the non-linear optimization step, and computing discrete correspondences using kd-trees. It is unique in that it provides symmetry and incorporates the structural assumptions of [7]. Because closest point look up is done with euclidean distance, however, kd-trees can be used to achieve fast performance on large pointclouds. This is typically not possible with fully probabilistic methods as these require computing a MAP estimate over assignments. In contrast to [8], we argue that the data should be assumed to be locally planar since most environments sampled for range data are piecewise smooth surfaces. By giving the minimization processes a probabilistic interpretation, we show that is easy to extend the technique to include structural information from both scans, rather then just one as is typically done in "point-to-plane" ICP. We show that introducing this symmetry improves accuracy and decreases dependence on parameters.

Unlike the IDC [15] and MbICP [16] algorithms, our approach is designed to deal with large 3D pointclouds. Even more fundamentally both of these approaches are somewhat orthogonal to our technique. Although MbICP suggests an alternative distance metric (as do we), our metric aims to take into account structure rather then orientation. Since our technique does not rely on any particular type (or number) of correspondences, it would likely be improved by incorporating a secondary set of correspondences as in IDC.

A key difference between our approach and [17] is the computational complexity involved. [17] is designed to deal with planar scan data – the Generalized Hough Transform suggested requires comparing every point in one scan with every point in the other (or a proportional number of comparisons in the case of sampling). Our approach works with kd-trees for closest point look up and thus requires $O(n \log(n))$ explicit point comparisons. It is not clear how to efficiently generalize the approach in [17] to the datasets considered in this paper. Furthermore, there are philosophical differences in the models.

This paper proceeds by summarizing the ICP and point-to-plane algorithms, and then introducing Generalized-ICP as a natural extension of these two standard approaches. Experimental results are then presented which highlight the advantages of Generalized-ICP.

A. ICP

The key concept of the standard ICP algorithm can be summarized in two steps:

1) compute correspondences between the two scans.
2) compute a transformation which minimizes distance between corresponding points.

Iteratively repeating these two steps typically results in convergence to the desired transformation. Because we are violating the assumption of full overlap, we are forced to add a maximum matching threshold d_{max}. This threshold accounts for the fact that some points will not have any correspondence in the second scan (e.g. points which are outside the boundary of scan A). In most implementations of ICP, the choice of d_{max} represents a trade off between convergence and accuracy. A low value results in bad convergence (the algorithm becomes "short sighted"); a large value causes incorrect correspondences to pull the final alignment away from the correct value. Standard ICP is listed as Alg. 1.

---

input : Two pointclouds: $A = \{a_i\}, B = \{b_i\}$
        An initial transformation: T_0
output: The correct transformation, T, which aligns A
        and B
1   $T \leftarrow T_0$;
2   **while** *not converged* **do**
3   **for** $i \leftarrow 1$ **to** N **do**
4          $m_i \leftarrow \texttt{FindClosestPointInA}(T \cdot b_i)$;
5   **if** $||m_i - T \cdot b_i|| \leq d_{max}$ **then**
6             $w_i \leftarrow 1$;
7   **else**
8             $w_i \leftarrow 0$;
9   **end**
10   **end**
11     $T \leftarrow \underset{T}{\operatorname{argmin}} \{\sum_i w_i ||T \cdot b_i - m_i||^2\}$;
12 **end**

Algorithm 1: Standard ICP

B. Point-to-plane

The point-to-plane variant of ICP improves performance by taking advantage of surface normal information. Originally introduced by Chen and Medioni[7], the technique has come into widespread use as a more robust and accurate variant of standard ICP when presented with 2.5D range data. Instead of minimizing $\Sigma||T \cdot b_i - m_i||^2$, the point-to-plane algorithm minimizes error along the surface normal (i.e. the projection of $(T \cdot b_i - m_i)$ onto the sub-space spanned by the surface normal). This improvement is implemented by changing line 11 of Alg. 1 as follows:

$$T \leftarrow \underset{T}{\operatorname{argmin}} \{\sum_i w_i ||\eta_i \cdot (T \cdot b_i - m_i)||^2\}$$

where η_i is the surface normal at m_i.

III. GENERALIZED-ICP

A. Derivation

Generalized-ICP is based on attaching a probabilistic model to the minimization step on line 11 of Alg. 1. The technique keeps the rest of the algorithm unchanged so as to reduce complexity and maintain speed. Notably, correspondences are still computed with the standard Euclidean distance rather then a probabilistic measure. This is done to allow for the use of kd-trees in the look up of closest points and hence maintain the principle advantages of ICP over other fully probabilistic techniques – speed and simplicity.

Since only line 11 is relevant, we limit the scope of the derivation to this context. To simplify notation, we assume that the closest point look up has already been performed and that the two point clouds, $A = \{a_i\}_{i=1,...,N}$ and $B = \{b_i\}_{i=1,...,N}$, are indexed according to their correspondences (i.e. a_i corresponds with b_i). For the purpose of this section, we also assume all correspondences with $||m_i - T \cdot b_i|| > d_{max}$ have been removed from the data.

In the probabilistic model we assume the existence of an underlying set of points, $\hat{A} = \{\hat{a}_i\}$ and $\hat{B} = \{\hat{b}_i\}$, which generate A and B according to $a_i \sim \mathcal{N}(\hat{a}_i, C_i^A)$ and $b_i \sim \mathcal{N}(\hat{b}_i, C_i^B)$. In this case, $\{C_i^A\}$ and $\{C_i^B\}$ are covariance matrices associated with the measured points. If we assume perfect correspondences (geometrically consistent with no errors due to occlusion or sampling), and the correct transformation, $\mathbf{T}^*$, we know that

$$\hat{b}_i = \mathbf{T}^* \hat{a}_i \tag{1}$$

For an arbitrary rigid transformation, $\mathbf{T}$, we define $d_i^{(\mathbf{T})} = b_i - \mathbf{T}a_i$, and consider the distribution from which $d_i^{(\mathbf{T}^*)}$ is drawn. Since a_i and b_i are assumed to be drawn from independent Gaussians,

$$d_i^{(\mathbf{T}^*)} \sim \mathcal{N}(\hat{b}_i - (\mathbf{T}^*)\hat{a}_i, C_i^B + (\mathbf{T}^*)C_i^A(\mathbf{T}^*)^T)$$
$$= \mathcal{N}(0, C_i^B + (\mathbf{T}^*)C_i^A(\mathbf{T}^*)^T)$$

by applying Eq. (1).

Now we use MLE to iteratively compute $\mathbf{T}$ by setting

$$\mathbf{T} = \underset{\mathbf{T}}{\operatorname{argmax}} \prod_i p(d_i^{(\mathbf{T})}) = \underset{\mathbf{T}}{\operatorname{argmax}} \sum_i \log(p(d_i^{(\mathbf{T})}))$$

The above can be simplified to

$$\mathbf{T} = \underset{\mathbf{T}}{\operatorname{argmin}} \sum_i d_i^{(\mathbf{T})^T}(C_i^B + \mathbf{T}C_i^A\mathbf{T}^T)^{-1}d_i^{(\mathbf{T})} \tag{2}$$

This defines the key step of the Generalized-ICP algorithm.

The standard ICP algorithm can be seen as a special case by setting

$$C_i^B = I$$
$$C_i^A = 0$$

In this case, (2) becomes

$$\mathbf{T} = \underset{\mathbf{T}}{\operatorname{argmin}} \sum_i d_i^{(\mathbf{T})^T} d_i^{(\mathbf{T})}$$
$$= \underset{\mathbf{T}}{\operatorname{argmin}} \sum_i ||d_i^{(\mathbf{T})}||^2 \tag{3}$$

which is exactly the standard ICP update formula.

With the Generalized-IPC framework in place, however, we have more freedom in modeling the situation; we are free to pick any set of covariances for $\{C_i^A\}$ and $\{C_i^B\}$. As a motivating example, we note that the point-to-plane algorithm can also be thought of probabilistically.

The update step in point-to-plane ICP is performed as:

$$\mathbf{T} = \underset{\mathbf{T}}{\operatorname{argmin}} \left\{ \sum_i ||\mathbf{P_i} \cdot d_i||^2 \right\} \tag{4}$$

where $\mathbf{P_i}$ is the projection onto the span of the surface normal at b_i. This minimizes the distance of $\mathbf{T} \cdot a_i$ from the plane defined by b_i and its surface normal. Since $\mathbf{P_i}$ is an orthogonal projection matrix, $\mathbf{P_i} = \mathbf{P_i}^2 = \mathbf{P_i}^T$. This means $||\mathbf{P_i} \cdot d_i||^2$ can be reformulated as a quadratic form:

$$||\mathbf{P_i} \cdot d_i||^2 = (\mathbf{P_i} \cdot d_i)^T \cdot (\mathbf{P_i} \cdot d_i)$$
$$= d_i^T \cdot \mathbf{P_i} \cdot d_i$$

Looking at (4) in this format, we get:

$$\mathbf{T} = \underset{\mathbf{T}}{\operatorname{argmin}} \left\{ \sum_i d_i^T \cdot \mathbf{P_i} \cdot d_i \right\} \tag{5}$$

Observing the similarity between the above and (2), it can be shown that point-to-plane ICP is a limiting case of Generalized-ICP. In this case

$$C_i^B = \mathbf{P_i}^{-1} \tag{6}$$
$$C_i^A = 0 \tag{7}$$

Strictly speaking $\mathbf{P_i}$ is non-invertible since it is rank deficient. However, if we approximate $\mathbf{P_i}$ with an invertible $\mathbf{Q_i}$, Generalized-ICP approaches point-to-plane as $\mathbf{Q_i} \rightarrow \mathbf{P_i}$. We can intuitively interpret this limiting behavior as b_i being constrained along the plane normal vector with nothing known about its location inside the plane itself.

B. Application: plane-to-plane

In order to improve performance relative to point-to-plane and increase the symmetry of the model, Generalized-ICP can be used to take into account surface information from both scans. The most natural way to incorporate this additional structure is to include information about the local surface of the second scan into (7). This captures the intuitive nature of the situation, but is not mathematically feasible since the matrices involved are singular. Instead, we use the intuition of point-to-plane to motivate a probabilistic model.

The insight of the point-to-plane algorithm is that our point cloud has more structure then an arbitrary set of points in 3-space; it is actually a collection of surfaces sampled by a range-measuring sensor. This means we are dealing with
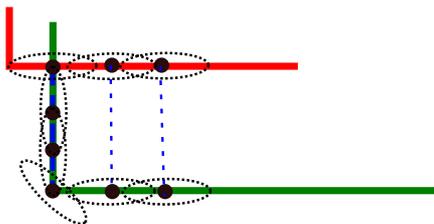
Fig. 1. illustration of plane-to-plane

a sampled 2-manifold in 3-space. Since real-world surfaces are at least piece-wise differentiable, we can assume that our dataset is locally planar. Furthermore, since we are sampling the manifold from two different perspectives, we will not in general sample the exact same point (i.e. the correspondence will never be exact). In essence, every measured point only provides a constraint along its surface normal. To model this structure, we consider each sampled point to be distributed with high covariance along its local plane, and very low covariance in the surface normal direction. In the case of a point with e_1 as its surface normal, the covariance matrix becomes

$$\begin{pmatrix} \epsilon & 0 & 0 \\ 0 & 1 & 0 \\ 0 & 0 & 1 \end{pmatrix}$$

where ϵ is a small constant representing covariance along the normal. This corresponds to knowing the position along the normal with very high confidence, but being unsure about its location in the plane. We model both a_i and b_i as being drawn from this sort of distribution.

Explicitly, given μ_i and ν_i – the respective normal vectors at b_i and a_i – C_i^B and C_i^A are computed by rotating the above covariance matrix so that the ϵ term represents uncertainty along the surface normal. Letting $\mathbf{R}_x$ denote one of the rotations which transform the basis vector $e_1 \to x$, set

$$C_i^B = \mathbf{R}_{\mu_i} \cdot \begin{pmatrix} \epsilon & 0 & 0 \\ 0 & 1 & 0 \\ 0 & 0 & 1 \end{pmatrix} \cdot \mathbf{R}_{\mu_i}^T$$

$$C_i^A = \mathbf{R}_{\nu_i} \cdot \begin{pmatrix} \epsilon & 0 & 0 \\ 0 & 1 & 0 \\ 0 & 0 & 1 \end{pmatrix} \cdot \mathbf{R}_{\nu_i}^T$$

The transformation, $\mathbf{T}$, is then computed via (2).

Fig. 1 provides an illustration of the effect of the algorithm in an extreme situation. In this case all of the points along the vertical section of the green scan are incorrectly associated with a single point in the red scan. Because the surface orientations are inconsistent, plane-to-plane will automatically discount these matches: the final summed covariance matrix of each correspondence will be isotropic and will form a very small contribution to the objective function relative to the thin and sharply defined correspondence covariance matrices. An alternative view of this behavior is as a soft constraint for each correspondence. The inconsistent matches allow the red scan-point to move along the x-axis while the green scan-points are

free to move along the y-axis. The incorrect correspondences thus form very weak and uninformative constraints for the overall alignment.

Computing the surface covariance matrices requires a surface normal associated with every point in both scans. There are many techniques for recovering surface normals from point clouds, and the accuracy of the normals naturally plays an important role in the performance of the algorithm. In our implementation, we used PCA on the covariance matrix of the 20 closest points to each scan point. In this case the eigenvector associated with the smallest eigenvalue corresponds with the surface normal. This method is used to compute the normals for both point-to-plane and Generalized-ICP. For Generalized-ICP, the rotation matrices are constructed so that the ϵ component of the variance lines up with the surface normal.[1]

IV. RESULTS

We compare all three algorithms to test performance of the proposed technique. Although efficient closed form solutions exist for $\mathbf{T}$ in standard ICP, we implemented the minimization with conjugate gradients to simplify comparison. Performance is analyzed in terms of convergence to the correct solution after a known offset is introduced between the two scans. We limit our tests to a maximum of 250 iterations for standard ICP, and 50 iterations for the other two algorithms since convergence was typically achieved before this point (if at all).

Both simulated (Fig. 3) and real (Fig. 4) data was used in order to demonstrate both theoretical and practical performance. The simulated data set also allowed tests to be performed on a wider range of environments with absolutely known ground truth. The outdoor simulated environment differs from the collected data primarily in the amount of occlusion presented, and in the more hilly features of the ground plane. The real-world outdoor tests also demonstrate performance with more detailed features and more representative measurement noise.

Simulated data was generated by ray-tracing a SICK scanner mounted on a rotating joint. Two 3D environments were created to test performance against absolute ground truth both in the indoor (Fig. 2(a)) and an outdoor (Fig. 2(b)) scenario. The indoor environment was based on an office hallway, while the outdoor setting reflects a typical landscape around a building. In both cases, we simulated a laser-scanner equipped robot traveling along a trajectory and taking measurements at fixed points along the path. Gaussian noise was added to make the tests more realistic.

Tests were also performed on real data from the logs of an instrumented car. The logs included data recorded by a roof-mounted Velodyne range finder as the car made a loop through a suburban environment and were annotated with GPS and IMU data. This made it possible to apply a pairwise constraint-based SLAM technique to generate ground truth

---

[1]In our implementation we compute these transformations by considering the eigen decomposition of the empirical covariance of the 20 closest points, $\hat{\boldsymbol{\Sigma}} = \mathbf{U}\mathbf{D}\mathbf{U}^T$. We then use $\mathbf{U}$ in place of the rotation matrix (in effect replacing $\mathbf{D}$ with $\mathbf{diag}(\epsilon, 1, 1)$ to get the final surface-aligned matrix).
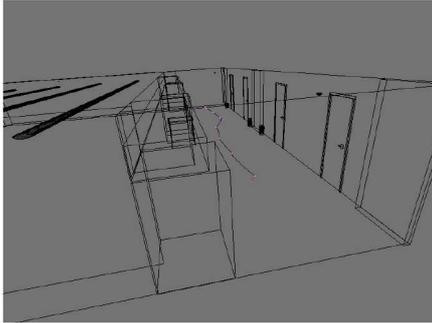
(a) indoor scene

(b) outdoor scene

Fig. 2.   simulated 3D environments
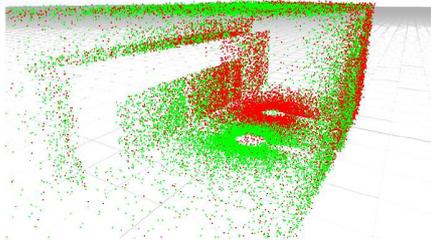
(a) indoor scene
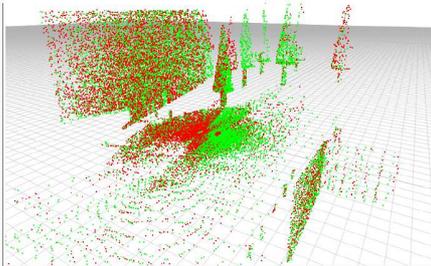
(b) outdoor scene

Fig. 3.   ray-traced scans – scan A is shown in green, scan B in red
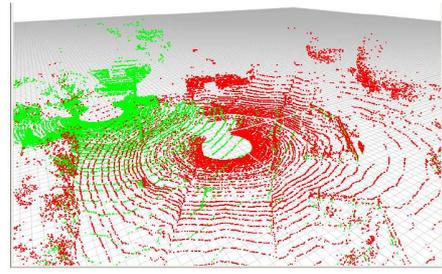
Fig. 4.   Velodyne scans – scan A is shown in green, scan B in red

positioning. Although (standard) ICP itself was used in the pairwise matching to generate the ground truth, the spacing of scans used for the SLAM approach was an order of magnitude smaller. In contrast, the scan pairs used for testing were extracted with much higher spacing (15-20+ meters) in order to pose a much more challenging problem. This is not a perfect method to generate ground truth, but we believe it provides a reasonable baseline to make comparisons between the algorithms.

To measure performance, all algorithms were run on pairs of scans from each of the three data sets. For each scan pair, the initial offset was set to the true offset with a uniformly generated error term added. The error term was set within ± 1.5m and $\pm 15°$ along all axes. Performance was measured by averaging positioning error over all scan pairs for a particular algorithm. In all cases tested, rotational error was negligible.

As mentioned before, selection of d_{max} plays an important role in the convergence of ICP. Fig. 5 shows the average error for different values of d_{max}; the plot shows average performance across all scan pairs. Fig. 9 shows the averages for individual scan pairs based on ideal values of d_{max}; it demonstrates the distribution of error across the range of scan pairs. In contrast to Fig. 5, the large number off random initial offsets averaged into each data point of Fig. 9 serves to sample the space of possible offsets. For Fig. 5, the algorithms were run on each scan pair with 10 randomly generated starting positions. For the plots in Fig. 9, each data point was generated with 50 random initial poses using best-case values for d_{max}. In all cases, error bars were computed as $\frac{\sigma}{\sqrt{N}}$.

The plots in Fig. 5 show that the proposed algorithm is more robust to choice of the matching threshold and demonstrates better performance in general. This is to be expected since it more completely models the environment and will automatically discount many incorrect matches based on the structure of the scene. In particular, Fig. 5 shows that in the simulated environments, the accuracy of the algorithm is not sensitive to overestimated values of d_{max}. For the real data, Generalized-ICP is still shown to be less sensitive due to the smaller slope of average error as $d_{max} \to \infty$. The discrepancy between simulated and real data can be explained by the difference in their respective frequency profiles. Whereas the simulated environments only have high-level features modeled

(a) simulated indoor

(b) simulated outdoor

(c) Velodyne data
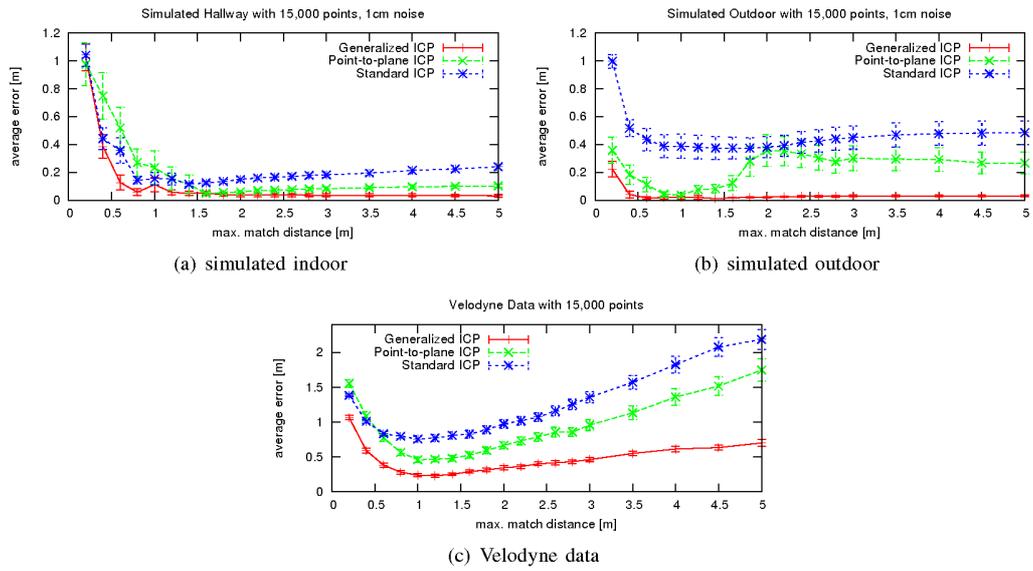
Fig. 5. average error as a function of d_{max}

(a) Initial alignment

(b) Point-to-plane

(c) Generalized-ICP
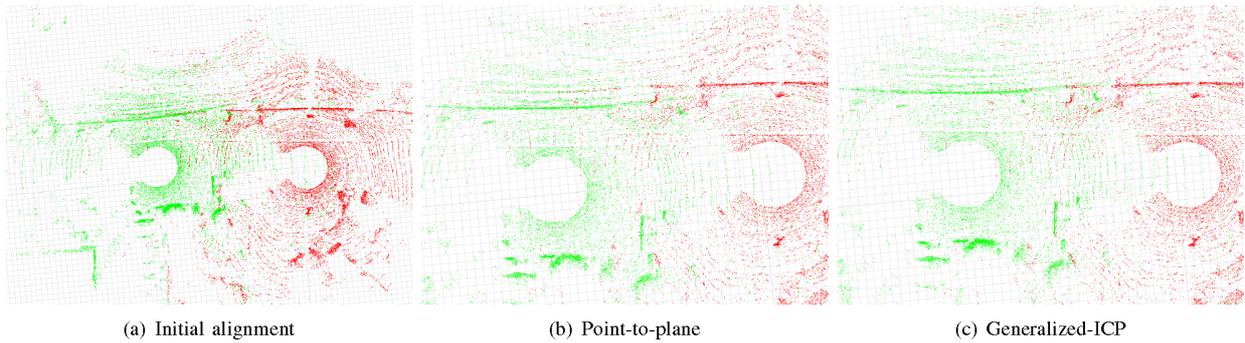
Fig. 6. Example of results for velodyne scan pair #31

(a) Initial alignment

(b) Point-to-plane

(c) Generalized-ICP
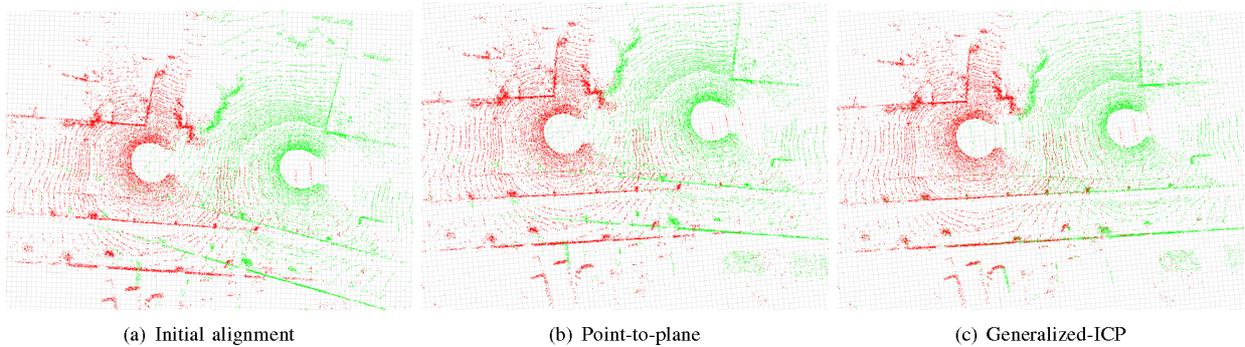
Fig. 7. Example of results for velodyne scan pair #45

(a) scan pair #31, view 1   (b) scan pair #31, view 2   (c) scan pair #45, view 1   (d) scan pair #45, view 2
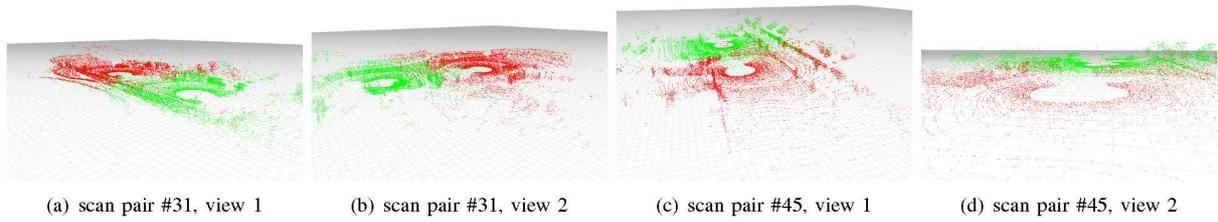
Fig. 8. Velodyne scan pairs #31 and #45 shown in perspective to illustrate scene complexity
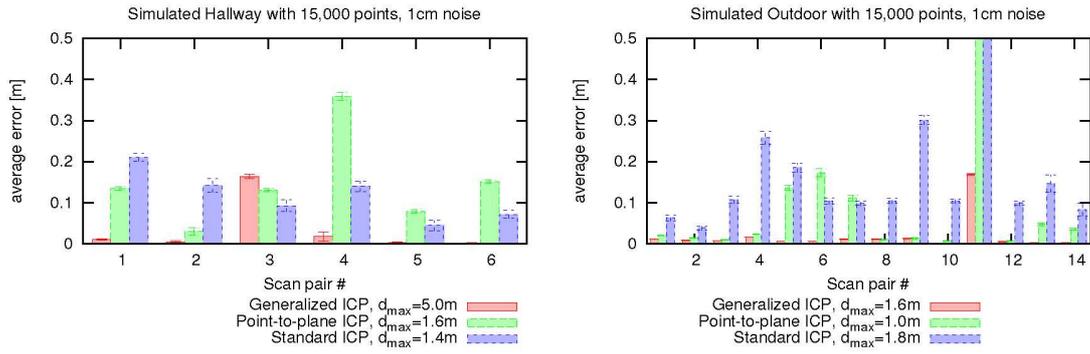
(a) simulated indoor   (b) simulated outdoor
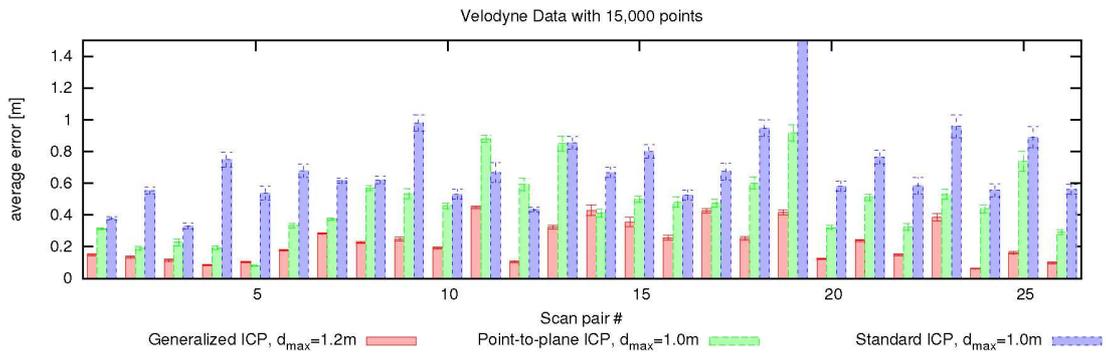
(c) Velodyne data #1 - #26
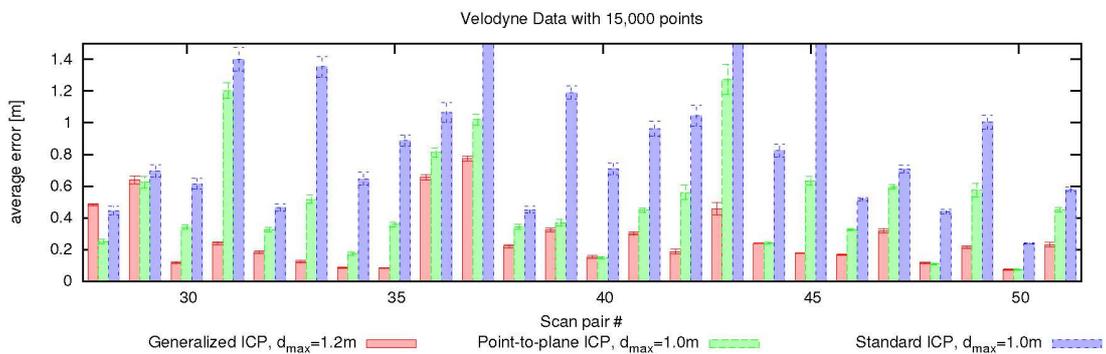

(d) Velodyne data #27 - #51

Fig. 9. average error with ideal values of d_{max} which minimize Fig. 5

by hand, the real world data contains much more detailed, high-frequency data. This increases the chances of incorrect correspondences which share a common surface orientation – a situation which is not taken into account by our algorithm. Nonetheless, even when comparing worst-cast values of d_{max} for Generalized-ICP with best-case values for point-to-plane, Generalized-ICP performs roughly as good.

As mentioned in Section II, the d_{max} plays an important role in the performance of ICP. Setting a low value decreases the chance of convergence, but increases accuracy. Setting a value which is too high increases the radius of convergence, but decreases accuracy since more incorrect correspondences are made. The algorithm proposed in this paper heavily reduces the penalty of picking a large value of d_{max} by discounting the effect of incorrect correspondences. This makes it easier to get good performance in a wide range of environment without hand-picking a value of d_{max} for each one.

In addition to the increased accuracy, the new algorithm gives equal consideration to both scans when computing the transformation. Fig. 6 and Fig. 7 show two situations where using the structure of both scans removed local minima which were present with point-to-plane. These represent top-down views of velodyne scans recorded approximately 30 meters apart and aligned. Fig. 8 shows some additional views of the same scan pairs to better illustrate the structure of the scene. The scans cover a range of 70-100 meters from the sensor in an outdoor environment as seen from a car driving on the road.

Because this minimization is still performed within the ICP framework, the approach combines the speed and simplicity of the standard algorithm with some of the advantages of fully probabilistic techniques such as EM. The theoretical framework also allows standard robustness techniques to be incorporated. For example, the Gaussian kernel can be mixed with a uniform distribution to model outliers. The Gaussian RVs can also be replaced by a distribution which takes into account a certain amount of slack in the matching to explicitly model the inexact correspondences (by assigning the distribution of $d_i^{(\mathbf{T})}$ a constant density on some region around 0). Although we have considered some of these variations, none of them have an obvious closed form which is easily minimized. This makes them too complex to include in the current work, but a good topic for future research.

V. Conclusion

In this paper we have proposed a generalization of the ICP algorithm which takes into account the locally planar structure of both scans in a probabilistic model. Most of the ICP framework is left unmodified so as to maintain the speed and simplicity which make this class of algorithms popular in practice; the proposed generalization only deals with the iterative computation of the transformation. We assume all measured points are drawn from Gaussians centered at the true points which are assumed to be in perfect correspondence. MLE is then used to iteratively estimate transformation for aligning the scans. In a range of both simulated and real-world experiments, Generalized-ICP was shown to increase accuracy. At the same time, the use of structural information from both scans decreased the influence of incorrect correspondences. Consequently the choice of maximum matching distance as a parameter for the correspondence phase becomes less critical to performance. These modifications maintain the simplicity and speed of ICP, while improving performance and removing the trade off typically associated with parameter selection.

References

[1] P. Besl, N. McKay. "A Method for Registration of 3-D Shapes," IEEE Trans. on Pattern Analysis and Machine Intel., vol. 14, no. 2, pp. 239-256, 1992.
[2] P. Biber, S. Fleck, W. Strasser. "A Probabilistic Framework for Robust and Accurate Matching of Point Clouds," Pattern Recognition, Lecture Notes in Computer Science, vol. 3175/2004, pp. 280-487, 2004.
[3] N. Gelfan, L. Ikemoto, S. Rusinkiewicz, M. Levoy. "Geometrically Stable Sampling for the ICP Algorithm," Fourth International Conference on 3-D Digital Imaging and Modeling, p. 260, 2003.
[4] D. Haehnel, W. Burgard. "Probabilistic Matching for 3D Scan Registration," Proc. of the VDI-Conference Robotik, 2002.
[5] Z. Zhang. "Iterative Point Matching for Registration of Free-Form Curves," IRA Rapports de Recherche, Programme 4: Robotique, Image et Vision, no. 1658, 1992.
[6] D. Hahnel, W. Burgard, S. Thrun. "Learning compact 3D models of indoor and outdoor environments with a mobile robot," Robotics and Autonomous Systems, vol. 44, pp. 15-27, 2003.
[7] Y. Chen, G. Medioni. "Object Modeling by Registration of Multiple Range Images," Proc. of the 1992 IEEE Intl. Conf. on Robotics and Automation, pp. 2724-2729, 1991.
[8] L. Montesano, J. Minguez, L. Montano. "Probabilistic Scan Matching for Motion Estimation in Unstructured Environments," IEEE Intl. Conf. on. Intelligent Robots and Systems, pp. 3499-3504, 2005.
[9] A. Fitzgibbon. "Robust registration of 3D and 3D point sets," Image and Vision Computing, vol. 21, no. 13-14, pp. 1145-1153, 2003.
[10] B. Horn. "Closed-form solution of absolute orientation using unit quaternions," Journal of the Optical Society of America A, vol. 4, pp. 629-642, 1987.
[11] S. Rusinkiewicz, M. Levoy. "Efficient Variants of the ICP Algorithm," Third International Conference on 3-D Digital Imaging and Modeling, p. 145, 2001.
[12] G. Dalley, P. Flynn. "Pair-Wise Range Image Registration: A Study in Outlier Classification," Computer Vision and Image Understanding, vol. 87, pp. 104-115, 2002.
[13] S. Kim , Y. Hwang , H. Hong , M. Choi. "An Improved ICP Algorithm Based on the Sensor Projection for Automatic 3D Registration," Lecture Notes in Computer Science, vol. 2972/2004 pp. 642-651, 2004.
[14] J.-S. Gutmann, C. Schlegel, "AMOS: comparison of scan matching approaches for self-localization in indoor environments," eurobot, p.61, 1st Euromicro Workshop on Advanced Mobile Robots (EUROBOT), 1996.
[15] F. Lu, E. Milos. "Robot Pose Estimation in Unknown Environments by Matching 2D Range Scans," Journal of Intelligent Robotics Systems 18: pp. 249-275, 1997.
[16] J. Minguez, F. Lamiraux, L. Montesano. "Metric-Based Scan Matching Algorithms for Mobile Robot Displacement Estimation," Robotics and Automation, Proceedings of the 2005 IEEE International Conference on, pp. 3557-3563, 2005.
[17] A. Censi, "Scan matching in a probabilistic framework," Robotics and Automation, Proceedings of the 2006 IEEE International Conference on, pp. 2291-2296, 2006.
[18] K. Pulli, "Mutliview Registration for Large Data Sets," 3-D Digital Imaging and Modeling, 1999. Proceedings. Second International Conference on, pp. 160-168, 1999.